Modeling and Control of a Variable-Speed Constant-Frequency Synchronous Generator With Brushless Exciter

Chunting Mi, *Senior Member, IEEE*, Mariano Filippa, *Student Member, IEEE*, John Shen, and Narashim Natarajan

***Abstract*—This paper presents the modeling, control, and implementation of a novel variable-speed constant-frequency power generation system for renewable and distributed energy applications. The generation system consists of a wound-rotor generator, a brushless exciter and a low-rating controlled power converter. The main generator is a doubly fed induction machine which is operated as a synchronous generator. The advantages of the proposed system are reduced harmonic injection to power grid, wide speed operation range covering both subsynchronous and super-synchronous speeds, self var support, and increased reliability. It can be directly applied to wind power generators, small-scale hydroelectric generators, stand-alone diesel and gasoline generators, and aerospace and naval power generation systems where a variable speed turbine/engine is employed. An equivalent circuit model of a doubly fed generator was developed incorporating stator and rotor iron losses. Then the control of a standalone generation system is developed based on the mathematical model. Detailed implementation procedure is given. An experimental system and its control were implemented using an embedded real-time digital signal processor. Measurements of the experimental system validated the system design and readiness for prototyping in a relatively large power range.**

***Index Terms*—AC generators, brushless, doubly fed, induction generators, modeling, permanent-magnet exciter, synchronous generator excitation, synchronous generators, variable-speed constant-frequency generator.**

I. Introduction

THERE has been increased interest in renewable and distributed power generation systems in recent years. Most of such power generation systems demand low-cost reliable generators suitable for variable-speed operation. In addition, in modern wind and small hydropower generation systems, the turbine designs are moving toward variable-speed architectures to increase energy capture capability [1].

There are two major categories of variable-speed power generation systems [2], [3]. The first category is a variable-frequency generator, either a squirrel-cage induction machine, or a wound-field synchronous machine, or a permanent-magnet (PM) synchronous machine, all using full-power-rating pulsewidth-modulation (PWM) converters, as shown in Fig. 1(a). The second category is a variable-speed constant-frequency generation system which uses a doubly fed induction generator and a reduced-rating power converter, as shown in Fig. 1(b). The former offers simple configurations for generators but employs expensive power electronics converters. If a squirrel-cage induction generator is in place, it must be connected to a stable voltage source for excitation and reactive power (var) support. The secondary, doubly fed wound-rotor induction machines, require brushes and slip rings which increase maintenance work. As these systems are usually located in remote mountainous areas, it is important to have a robust maintenance-free system. Moreover, all conversion schemes suffer from harmonic distortion caused by power electronic converters directly connected to the power grid.

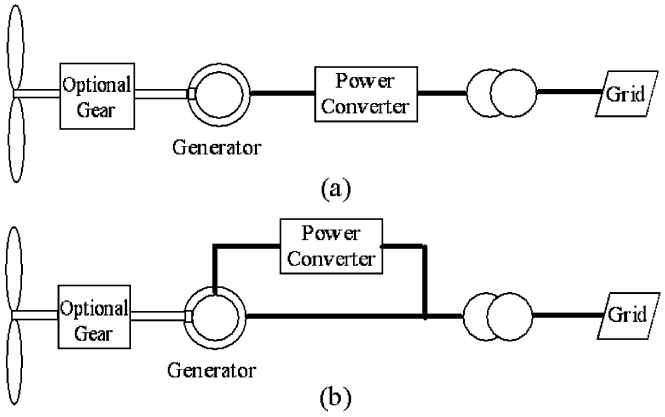

Fig. 1. Traditional wind power generation systems. (a) Variable-frequency generator with full-rating power converter. (b) Doubly fed induction generator with reduced-rating power converter.

A cascaded induction machine was proposed to eliminate the slip rings and brushes [4]. It showed that harmonic distortion could be reduced but the cost of the system was significantly increased and the system efficiency dropped. Doubly fed reluctant generators were also studied [5]. It showed that the size of a doubly fed reluctant generator was considerably larger than the size of an induction or synchronous machine with the same power rating. A doubly fed induction generator similar to a doubly fed reluctant generator was also proposed by Brune *et al.* [6].

This paper proposes a novel variable-speed constant-frequency power generation system suitable for renewable and distributed energy systems. The objective is to improve power quality, increase the system reliability, and eliminate the dependence on any external active or reactive power support.

Paper IPCSD 03–125, presented at the 2003 Industry Applications Society Annual Meeting, Salt Lake City, UT, October 12–16, and approved for publication in the IEEE TRANSACTIONS ON INDUSTRY APPLICATIONS by the Electric Machines Committee of the IEEE Industry Applications Society. Manuscript submitted for review June 19, 2003 and released for publication November 29, 2003. This work was supported by the Faculty Summer Research Grant at the University of Michigan, Dearborn.

The authors are with the Department of Electrical and Computer Engineering, University of Michigan, Dearborn, MI 48128 USA (e-mail: chrismi@umich.edu).

Digital Object Identifier 10.1109/TIA.2004.824504

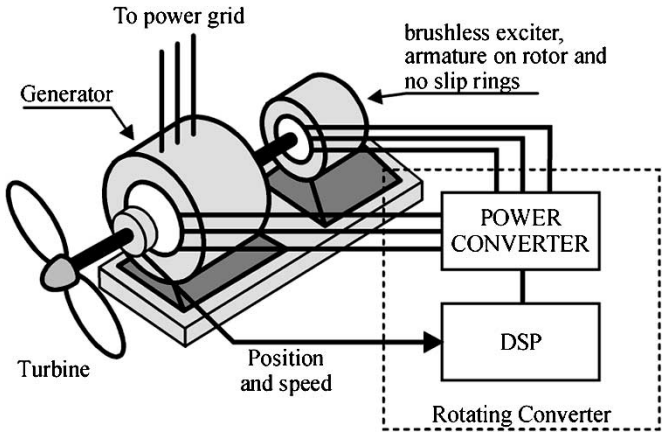

Fig. 2. System configuration of the proposed variable-speed constant-frequency power generation system.

An equivalent circuit model was developed for the proposed generation system using doubly fed generators, incorporating stator and rotor iron losses. Experiments were carried out on a stand-alone system to validate the system design and analysis.

II. System Description

The proposed power generation system is shown in Fig. 2. The system consists of a main wound-rotor generator, with the shaft connected to the wind turbine and the wound-rotor winding connected to the armature of the exciter; a brushless exciter (with permanent-magnet poles or field windings) with field on the stator and armature windings on the rotor; a low-rating rotating power converter constructed to rotate with the main shaft. The configuration of the main generator in Fig. 2 is identical to a doubly fed wound-rotor induction machine. Due to the way the machine is controlled, it is more suitable to name it a synchronous machine [8].

Suppose the machine is running at rotor speed ω_m, and the required frequency of the output is ω_1, the rotor winding must produce a magnetic field at the speed equal to "$(p/2)\omega_{\rm m} - \omega_1$," where p is the number of poles. This air-gap field generated by the rotor winding must be able to produce the required stator terminal voltage. When the generator is loaded, the exciter should be able to provide additional current to overcome the stator armature reaction in order to maintain the required stator terminal voltage. It will also be shown later, that the exciter must be able to be operated either in generating mode (subsynchronous speed) or motoring mode (super-synchronous speed).

III. Modeling of the Main Generator Using Equivalent Circuit Approach

Doubly fed induction machines have been extensively studied in the past [7]–[15]. In these studies, almost all of the equivalent circuits of doubly fed induction generator used induction motor convention. In particular, Concordia *et al.* [7] suggested that rotor phasors in the equivalent circuit for super-synchronous operation should be the conjugate of the actual phasors.

This paper presents an equivalent circuit model for the proposed main generator suitable for both subsynchronous and super-synchronous speed operation using a generator convention and incorporating stator and rotor iron losses.

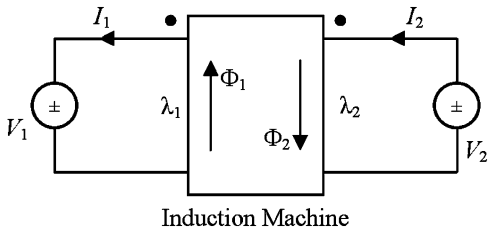

Fig. 3. Polarity mark of the generator [14]. A current entering a polarity-marked terminal produces an MMF and flux that is in a positive direction ($I_2 \rightarrow \Phi_2$). A current flowing out of a polarity-marked terminal produces a mmf and flux in the negative direction ($I_1 \rightarrow \Phi_1$). Therefore, I_1 generates a negative flux linkage on both the stator and the rotor windings, but rotor current I_2 generates a positive flux linkage in both the stator and the rotor windings. It has been shown in (6) and (7).

A. Voltage and Current of the Main Generator

Under steady-state operation, the stator voltage and current of phase A of the main generator can be expressed as

$$v_1(t) = \sqrt{2}V_1\cos(\omega_1 t)$$
$$i_1(t) = \sqrt{2}I_1\cos(\omega_1 t - \varphi_1) \quad (1)$$

where φ_1 is the power factor angle of the stator, and ω_1 is the frequency of the stator current which is assumed to be the constant synchronous frequency. Subscript 1 donates the stator quantities.

Similarly, the voltage and current of rotor phase a of the main generator can be expressed as

$$v_2(t) = \sqrt{2}V_2\cos(\omega_2 t + \theta)$$
$$i_2(t) = \sqrt{2}I_2\cos(\omega_2 t + \theta - \varphi_2) \quad (2)$$

where φ_2 is the power factor angle of the rotor, ω_2 is the frequency of rotor voltage and current, $\omega_2 = \omega_1 - \omega_m = s\omega_1$, s is the rotor slip, $\omega_{\rm m}$ is the actual rotor mechanical angular speed, and θ is the angle between stator voltage and rotor voltage. When referred to the rotating frame $(d\text{-}q)$ system, θ is similar to the power angle of a synchronous machine.

Both the stator and the rotor quantities can be expressed as phasors

$$V_1 = V_1 e^{j0} \quad I_1 = I_1 e^{j\varphi_1} \quad V_2 = V_2 e^{j0} \quad I_2 = I_2 e^{j\varphi_2}. \quad (3)$$

B. Equivalent Circuit in the Stationary Stator Frame

In grid-connected doubly fed machines, there are voltage sources connected to both the stator and the rotor. When a synchronous generator convention is used, rotor currents flow into the machine and the stator current flows out the machine, as shown in Fig. 3 [16].

By using the definitions given in Fig. 3, the voltage and flux linkage equations per phase of the doubly fed machine can be written as follows [17]:

$$p\lambda_1 = r_1 I_1 + V_1 \quad (4)$$
$$V_2 = r_2 I_2 + p\lambda_2 \quad (5)$$
$$\lambda_1 = -L_1 I_1 + L_m I_2 \quad (6)$$
$$\lambda_2 = -L_m I_1 + L_2 I_2. \quad (7)$$

The voltage equation can be derived by substituting (6) and (7) into (4) and (5)

$$V_1 + I_1 r_1 = -j\omega_1 L_1 I_1 + j\omega_1 L_m I_2 \quad (8)$$
$$V_2 = I_2 r_2 + j\omega_2 L_2 I_2 - j\omega_2 L_m I_1. \quad (9)$$

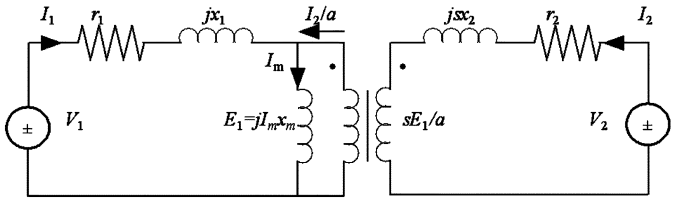

Fig. 4. Equivalent circuit at subsynchronous speed following generator convention. The excitation is from the rotor, which generates an induced voltage at the right side of the ideal transformer.

Since $\omega_2 = s\omega_1$ the rotor voltage equation becomes

$$V_2 = I_2 r_2 + js \cdot \omega_1 L_2 \cdot I_2 - js \cdot \omega_1 L_m \cdot I_1. \tag{10}$$

Further, by introducing the effective stator/rotor turns ratio a, stator voltage (8) can be reorganized as

$$\begin{aligned} V_1 + I_1 r_1 &= -j\omega_1 (L_1 - aL_m) I_1 + j\omega_1 a L_m \left(\frac{I_2}{a} - I_1 \right) \\ &= -jx_1 I_1 + E_1 \\ Or \quad E_1 &= V_1 + I_1 r_1 + jx_1 I_1 \end{aligned} \tag{11}$$

and rotor voltage (9) can be reorganized as

$$\begin{aligned} V_2 &= I_2 r_2 + js\omega_1 \left(L_2 - \frac{L_m}{a} \right) I_2 + j \left(\frac{s}{a} \right) \omega_1 a L_m \left(\frac{I_2}{a} - I_1 \right) \\ &= I_2 r_2 + jsx_2 I_2 + \frac{sE_1}{a} \end{aligned} \tag{12}$$

where $x_1 = \omega_1(L_1 - aL_m)$, $x_2 = \omega_1(L_2 - L_m/a)$, $x_m - \omega_1 a L_m$, and $E_1 = jw_1 a L_m I_m$, $I_m = I_2/a - I_1$.

The equivalent circuit of a doubly fed machine can then be derived from (11) and (12), as shown in Fig. 4. The rotor and stator are linked by an ideal transformer with ratio of s/a, where slip s transfers rotor and stator frequency.

C. Super-Synchronous Speed

In the above derivation of the equivalent circuit, slip s was assumed to be positive as the generator is operated at subsynchronous speeds. The generator may be operated at super-synchronous speed or negative slip s. If the equivalent circuit of Fig. 4 is used, both sE_1/a and sx_2 in the rotor circuit become negative. Rotor frequency $\omega_2 = s\omega_1$ is also negative due to negative slip. In the real word, it is preferable to express frequency as a positive number, e.g., $\omega_2 = |s|\omega_1$.

Since the air-gap field is still running at synchronous speed, the rotor winding sees a negative field because the actual rotor speed is higher than synchronous speed. As explained in Fig. 5, the flux linkage can now be expressed as

$$\lambda_1 = -L_1 I_1 + L_m I_2 \tag{13}$$

$$-\lambda_2 = -L_m I_1 + L_2 I_2. \tag{14}$$

It can be seen from (13) that the stator voltage equation is not affected by negative slip or negative-sequence rotor current. The

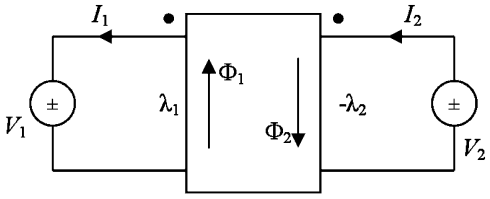

Fig. 5. Representation of the generator system at super-synchronous speed. The rotor current flows into the polarity-marked terminal producing a positive flux Φ_2. However, since the rotor is running at a speed higher than the air-gap field, the rotor sees a negative-sequence flux linkage. It is shown in (13) and (14).

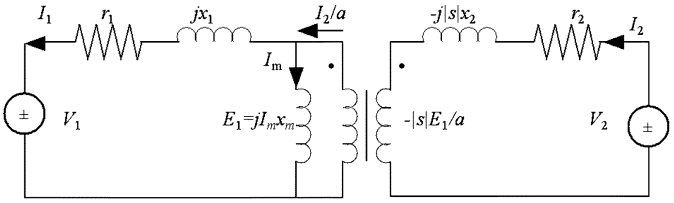

Fig. 6. Equivalent circuit at super-synchronous speed following generator convention.

rotor voltage equation, however, has to be revised according to (14)

$$\begin{aligned} V_2 &= I_2 r_2 + p\lambda_2 \\ &= I_2 r_2 - j\omega_2 L_2 I_2 + j\omega_2 L_m I_1 \\ &= I_2 r_2 - j|s|\omega_1 L_2 I_2 + j|s|\omega_1 L_m I_1 \\ &= I_2 r_2 - j|s|\omega_1 \left(L_2 - \frac{L_m}{a} \right) I_2 \\ &\quad - j \left(\frac{|s|}{a} \right) \omega_1 a L_m \left(\frac{I_2}{a} - I_1 \right) \end{aligned} \tag{15}$$

$$V_2 = I_2 r_2 - j|s| x_2 I_2 - \frac{|s| E_1}{a}. \tag{16}$$

The equivalent circuit for super-synchronous speed operation can be derived from (16) as shown in Fig. 6. Since $s < 0$, so $-|s|E_1/a = sE_1/a$, and $-|s|x_2 = sx_2$. Therefore, Fig. 6 and Fig. 4 are essentially the same.

Further analysis of the ideal transformer in Fig. 4 reveals that there is also a difference of power on the two sides of the ideal transformer. The real power on the rotor side of the ideal transformer is $\mathrm{Re}\{sE_1\ I_2^*/a\}$, but the real power transferred to the stator side of the ideal transformer is $\mathrm{Re}\{E_1\ I_2^*/a\}$. In Fig. 4, electric power transferred from V_2 to the stator is

$$\begin{aligned} P_2 &= \mathrm{Re}\{V_2 I_2{}^* - I_2 I_2{}^* r_2\} \\ &= \mathrm{Re}\{V_2 I_2{}^* - I_2 I_2{}^* r_2 - jI_2 I_2{}^* sx_2\} \\ &= \mathrm{Re}\{(V_2 - I_2 r_2 - jI_2 sx_2) I_2{}^*\} \\ &= \mathrm{Re}\left\{ \frac{sE_1 I_2{}^*}{a} \right\}. \end{aligned} \tag{17}$$

It can be seen from (17) that $\mathrm{RE}\{sE_1\ I_2^*/a\}$ does represent the electric power transferred from V_2 to the stator. The difference of the power on the two sides of the ideal transformer must represent the mechanical power on the shaft, which can be written as

$$P_m = \mathrm{Re}\left\{ \frac{(1-s) E_1 I_2{}^*}{a} \right\}. \tag{18}$$

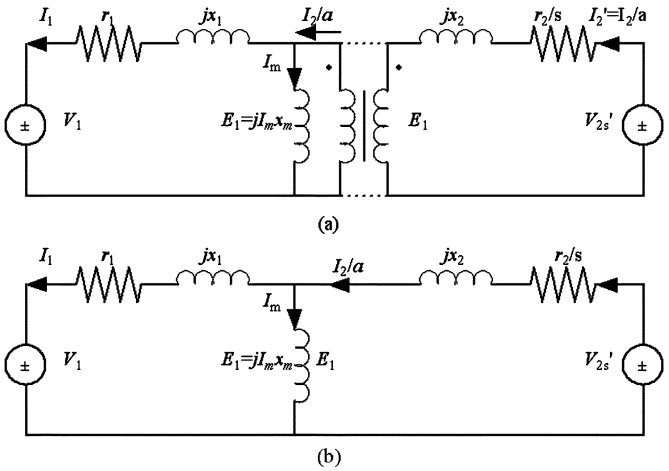

Fig. 7. Equivalent circuit of a doubly fed induction machine referred to the stator side. (a) Rotor quantities are transformed to the stator side. Since the voltage on both sides of the ideal transformer is equal, the rotor circuit can be connected with the stator circuit. (b) Further, since $I_2' = I_2/\mathrm{a}$, the ideal transformer can be eliminated.

D. Generalized Form of Equivalent Circuit

The equivalent circuit presented in Fig. 4 or Fig. 6 is convenient to use since the circuits use the actual magnitude and frequency of stator and rotor quantities, hence, no transformation is needed.

Shaft mechanical power is not included in Fig. 4. Sometimes, it may be more convenient to include the shaft mechanical power in the rotor circuit. This can be achieved by transferring rotor quantities to the stator side or vise versa.

Multiplying (12) by a/s, the rotor equation becomes

$$\frac{V_2'}{s} = I_2'\frac{r_2'}{s} + jx_2'I_2' + E_1 \tag{19}$$

where $V_2' = aV_2$, $I_2' = I_2/a$, $r_2' = a^2r_2$, $x_2' = a^2x_2$.

The new equivalent circuit can be derived from (19) as shown in Fig. 7.

The above transformation not only results in the change of the equivalent circuit, but also results in a change of power represented by each component in the rotor circuit. Note that the rotor power factor angle has not changed since $\varphi_2 = \tan^{-1}((r_2'/s)/(x_2')) = \tan^{-1}((r_2)/(sx_2))$.

The apparent power presented by each of the rotor components in Fig. 7 are

$$\frac{V_2'}{s}\cdot I_2'^{*} = \frac{V_2I_2^{*}}{s} = V_2I_2^{*} + \frac{1-s}{s}V_2I_2^{*} \tag{20}$$

$$I_2'^{2}\frac{r_2'}{s} = \left(\frac{I_2}{a}\right)^2\frac{a^2r_2}{s} = \frac{I_2^2r_2}{s} = I_2^2r_2 + \frac{1-s}{s}I_2^2r_2. \tag{21}$$

It can be seen from (20)–(22) that the power represented by each component of Fig. 7 now includes two terms.

In Fig. 7, the total real power transferred to the stator can be found by subtracting (21) from (20). By reorganizing, P_2 can be written as

$$P_2 = \mathrm{Re}\left\{V_2I_2^{*} - I_2I_2^{*}r_2\right\} + \frac{1-s}{s}\mathrm{Re}\left\{V_2I_2^{*} - I_2I_2^{*}r_2\right\}. \tag{22}$$

Comparing (22) to (17), it can be seen that the first term of (22) represents the electric power transferred to the stator by V_2. The second term in (22) can be reorganized using (17)

$$\frac{1-s}{s}\mathrm{Re}\left(V_2I_2^{*} - I_2I_2^{*}r_2\right) = (1-s)\mathrm{Re}\left(\frac{E_1I_2^{*}}{a}\right). \tag{23}$$

Comparing (23) to (18), it can be seen that the second term of (22), or the difference of real power of V_2'/s and (r_2'/s) represents the mechanical power transferred from rotor shaft to the stator.

E. Iron Losses

The equivalent circuit shown in Figs. 4, 6, and 7 do not include iron losses. The usual method to account for iron losses in induction machines is to have a resistance r_{ms} in parallel or series with the magnetizing reactance x_m, where r_{ms} represents the equivalent stator iron losses [16]. Rotor iron loss of induction machines is usually neglected due to the fact that the frequency of the magnetic field in the rotor iron is very low. Since doubly fed induction machines may be operated at large slip, iron losses will exist in both the stator and the rotor, within which the latter is proportional to the frequency of rotor flux density. The inclusion of iron losses in the equivalent circuit is rather complicated but this must be taken into account as the efficiency of induction generators is of fundamental importance and affected by rotor iron loss at large slip operations.

Although rotor iron loss exists and affects the efficiency of variable speed wind generators, iron losses were neglected in many studies [6], [7], [9]–[13]. In [8], it was claimed that the rotor iron is a function of s and changes sign when s changes sign. It proposed to have the iron loss represented by a resistance in series with the rotor winding resistance. In [14], the rotor iron loss was simply not represented in the equivalent circuit. In fact, since iron loss always exist no matter the machine running at super or sub synchronous speed, iron loss should always be positive regardless of slip s.

It is also worth noting that rotor iron loss always presents as long as slip is not zero, regardless of rotor currents. Similar to the stator iron loss, which is related to excitation current but not the actual stator current, the rotor iron loss is proportional to excitation current but not the actual rotor current. Therefore, to incorporate stator and rotor iron losses in the equivalent circuit, two resistances can be added in series with x_{m} as commonly done in induction machines, one to represent stator iron loss and the other to represent the rotor iron loss. Since rotor iron loss is proportional to rotor slip, the equivalent resistance is therefore proportional to slip. The equivalent circuit can be drawn in Fig. 8, where r_{ms} corresponds to the iron loss of the stator and $r_{\mathrm{mr}}{}'$ corresponds to the iron losses of the rotor calculated at synchronous frequency, e.g., when the rotor is stalled, and is referred to the stator side.

The equivalent circuit presented in Fig. 8 has some advantages over the ideas presented in [8]. First, if rotor iron loss is represented by a resistor in series with rotor winding resistance as suggested in [8], then rotor iron loss would have been proportional to rotor current. As rotor iron loss is only proportional to the magnitude and the frequency of rotor flux densities, it should not be related to rotor currents. For example, rotor iron loss exists even when rotor is open circuited. Similarly, stator

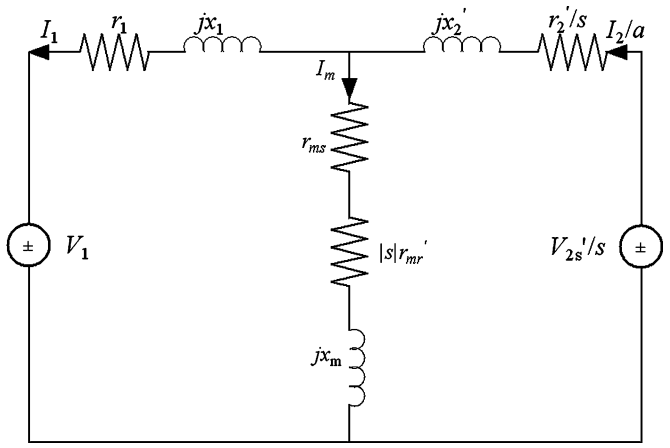

Fig. 8. Equivalent circuit of a doubly fed induction machine incorporating stator and rotor iron losses. Note the rotor iron loss is proportional to the rotor slip which results in an equivalent resistance proportional to rotor slip.

iron losses always exist no matter the excitation current is provided by the stator winding or by the rotor winding. Secondly, taking the absolute value of slip avoids reversing of the sign of rotor iron loss.

F. Rotor Voltage and Current

Wind turbines are designed to have an optimized speed–torque profile to provide maximum output power for any given wind speed. This means that, for a given wind speed, the turbine speed or slip is designed such that the output can be maximized. When the generation system is connected to an infinite bus, the generator terminal voltage is imposed by the infinite bus.

Therefore, for grid connected generators, the excitation frequency of the rotor voltage is determined by taking the difference of grid frequency and the actual rotor speed. The stator current can be predetermined for maximum power output corresponding to each wind speed. The corresponding V_2 can then be derived using V_1, I_1, $-\varphi_1$ and slip s for any particular wind speed, using the equivalent circuit of Fig. 8.

Let $z_1 = r_1 + jx_1$, $z_2 = r_2'/s + jx_2'$, $z_m = r_{ms} + |s|r_{mr} + jx_m$ then, for a given V_1, I_1, $-\varphi_1$ and slip s, the required V_2, I_2, and P_2 can be derived using the equivalent circuit shown in Figs. 8 and 4

$$V_2 = \frac{s}{a}\left[V_1\left(1+\frac{z_2'}{z_m}\right) + I_1 Z_1\left(1+\frac{z_2'}{z_1}+\frac{z_2'}{z_m}\right)\right] \quad (24)$$

$$I_2 = a\left[I_1\left(1+\frac{z_1}{z_m}\right)+\frac{V_1}{z_m}\right] \quad (25)$$

$$P_2 = \mathrm{Re}\left[I_2 * \mathrm{conj}(V_2)\right]. \quad (26)$$

For stand-alone systems, the power delivered is determined by the load connected to the generator. Therefore, I_2 is unknown. In this case V_2 can be controlled using a magnitude and frequency proportional–integral–differential (PID) controller, such that V_1 is maintained at constant magnitude and constant frequency, as shown in Fig. 9.

G. Relations of Input and Output Power

The power supplied by V_2 is

$$P_2 = \mathrm{Re}\left[V_2 {I_2}^*\right] = V_2 I_2 \cos(\varphi_2). \quad (27)$$

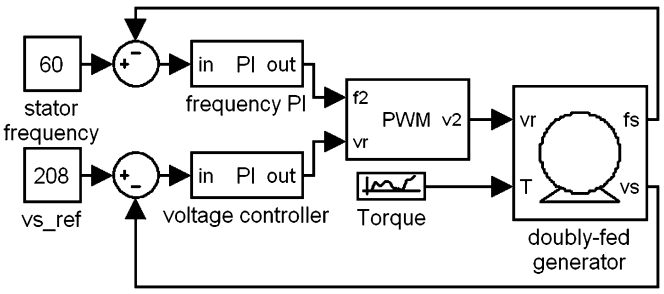

Fig. 9. Closed-loop control of a stand-alone system.

The power generated by the stator winding is

$$P_1 = \mathrm{Re}\left[V_1 {I_1}^*\right] = V_1 I_1 \cos(\varphi_1). \quad (28)$$

The difference between (28) and (27) gives the mechanical power delivered from the shaft to the air gap. In order to visualize the power flow in a doubly fed generator, let us neglect both rotor and stator resistance and leakage inductances. By using Fig. 4, the following equations can be derived:

$$\begin{aligned} P_1 &= V_1 I_1 \cos\varphi_1 \\ E_1 &= V_1 \\ V_2 &= \frac{sV_1}{a} \\ I_2 &= a\cdot\left[I_1\cos\varphi_1 + \frac{jV_1}{x_m} - jI_1\sin\varphi_1\right] \\ P_2 &= \mathrm{Re}\left(V_2 I_2^*\right) = sV_1 I_1\cos\varphi_1 = sP_1 \\ P_m &= P_1 - P_2 = (1-s)P_1 \end{aligned} \quad (29)$$

where P_1 is the output of the main generator, which is equal to the total shaft input from the turbine, P_{m} is the required mechanical power by the main generator, and P_2 is the power transferred through the exciter.

H. Power Flow in the Doubly Fed Machine

From (29), it can be seen that the power supplied by V_2 is proportional to slip s. Therefore, at subsynchronous speed, the rotor winding receives power and the exciter is running at generating mode. At super-synchronous speed, the rotor winding delivers power and the exciter is running at motoring mode.

Fig. 10 shows the direction of power flow in the machine. At subsynchronous speed, the total mechanical power from the wind turbine is $P_{\mathrm{M}} = P_1 = (1-s)P_1 + sP_1 = P_{\mathrm{m}} + sP_{\mathrm{m}}/(1-s)$, where sP_1 is electrical power produced by the exciter from the shaft mechanical power. The exciter is running at generator mode. This sP_1 is then supplied to the rotor winding of the main generator through the power converter.

The majority of the shaft power, $(1-s)P_1$, is directly transferred to electrical power through the air gap to the stator windings. The total electric power delivered at the stator terminals is equal to the mechanical power applied to the shaft, neglecting all losses, as shown in Fig. 10(a).

At super-synchronous speed, the total mechanical power from the turbine is $P_{\mathrm{M}} = P_1 = (1-|s|)P_1 + |s|P_1 = P_{\mathrm{m}} + |s|P_{\mathrm{m}}/(1-|s|)$, where $|s|P_1$ is transferred to electrical power by the rotor winding of the main generator, then delivered to the exciter through the power converter. The exciter is running in motoring mode. This portion of power is then

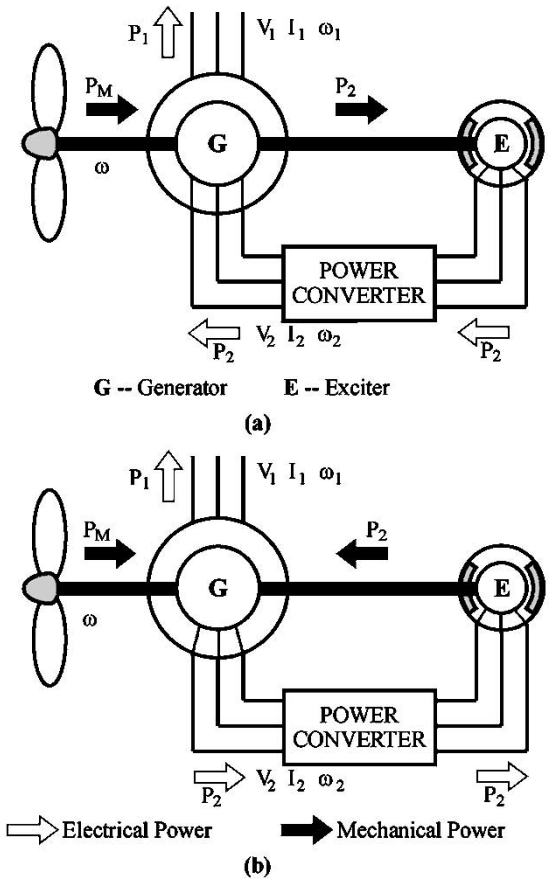

Fig. 10. Power flow in the proposed power generation system neglecting all losses of the system. (a) Subsynchronous speed, $s > 0, \omega < \omega_1$. Total power from the turbine is P_M, from which $(P_M - P_2)$ is used to drive the main generator; P_2 is used to drive the exciter; exciter output P_2 is supplied to the rotor of the main generator through the power converter. (b) Super-synchronous speed, $s < 0, \omega > \omega_1$. Total power from the turbine is P_M, and $(P_M + P_2)$ is used to drive the main generator where P_2 is supplied by the exciter; exciter input P_2 is supplied by the rotor winding of the main generator through the power converter.

transferred to mechanical power by the exciter to be applied on the shaft. The majority of the power, $(1 - |s|P_1)$, is directly transferred from the shaft to the air gap. The total electric power delivered at the stator terminals is again equal to the mechanical power on the shaft as shown in Fig. 10(b).

The efficiency of the main generator can be calculated by including all the losses of the generator as shown by (30), at the bottom of the page, where P_1, P_{ad}, and $P_{\rm mec}$, are output of the main generator, stray load loss, and friction and windage loss, respectively; I_1 and I_2 are the magnitude of stator and rotor current, respectively.

When losses of the system are included, the total output of the generator is equal to the total mechanical input minus all losses

$$P_1 = P_m - (p_g + p_e + p_c) \tag{31}$$

where p_g, p_e, and p_c are the losses of the generator, the exciter, and the rotating converter, respectively.

The system efficiency is

$$\eta = \frac{P_1}{P_m}. \tag{32}$$

IV. Exciter and Power Converter Rating

It can be seen from (29) that the required power by the rotor winding of the main generator is proportional to rotor slip and the total output of the main generator. The exciter power rating can be determined using (24)–(26). When neglecting all losses, it is approximated as

$$P_{2,\max} = \max\{|s|P_1\}. \tag{33}$$

The power converter must supply the rotor winding with both active and reactive power. Maximum apparent power supplied to the rotor winding is

$$S_{rotor} = \max\{|V_2 I_2\} = \max\{|s|V_1 I_1\}. \tag{34}$$

The maximum rotor current can be determined by (25).

When neglecting all losses, the maximum current needed for the power converter can be approximated as

$$I_2 = \max\left\{\sqrt{I_1^2 - 2\frac{V_1 I_1}{x_m}\sin\varphi_1 + \left(\frac{V_1}{x_m}\right)^2}\right\}. \tag{35}$$

V. Experimental Verification

A 2.2-kW 208-V four-pole 60-Hz experimental system was tested to validate the developed model. The equivalent circuit parameters of the main generator are shown in Table I. The system was operated as a stand-alone generation system simulating a wind power generator. The test bench consisted of main generator, which is made by a 3-hp induction machine and a stationary converter as shown in Fig. 11. The exciter was substituted by a dc bus. There is an encoder connected to the main shaft to measure the speed of the machine.

The main generator can be modeled using the proposed equivalent circuit using the parameters shown in Table I. The calculated exciter and power converter rating are shown in Table II for a given wind turbine profile. It can be seen from Table II that, given the stator voltage and frequency, the maximum power required for the exciter is 0.936 kW at motoring mode. The maximum power converter power rating is 1.5 kVA and maximum voltage is 127 V.

The control of the system was implemented using a digital signal processor (DSP) embedded real-time controller, as shown in Fig. 12. The stator voltage feedback was acquired through the two ADC channels of the DSP. The stator voltage is controlled using a voltage PI controller. The required frequency of rotor excitation is obtained by taking the difference of the expected stator frequency and the rotor angular speed converted to electrical degrees. The required gating for the rotor excitation was generated based on these two inputs.

$$\eta_G = \frac{P_1}{P_1 + 3I_1^2 r_1 + 3I_2^2 r_2 + 3I_m^2 (r_m + r_{ms} + |s|r_{mr}) + p_{ad} + p_{\rm mec}} \tag{30}$$

TABLE I
EQUIVALENT CIRCUIT PARAMETERS OF THE EXPERIMENTAL MOTOR

Name	Symbol	Value
Stator resistance (Ohms)	r_1	0.41
Stator leakage inductance (mH)	L_1	3.2
Stator iron loss component (Ohms)	r_{ms}	0.63
Rotor iron loss component (Ohms)	r_{mr}	0.08
Mutual inductance (mH)	L_m	53.7
Rotor resistance (Ohms)	r_2	1.18
Rotor leakage inductance (mH)	L_2	2.7
Stator/rotor turns ratio	a	1

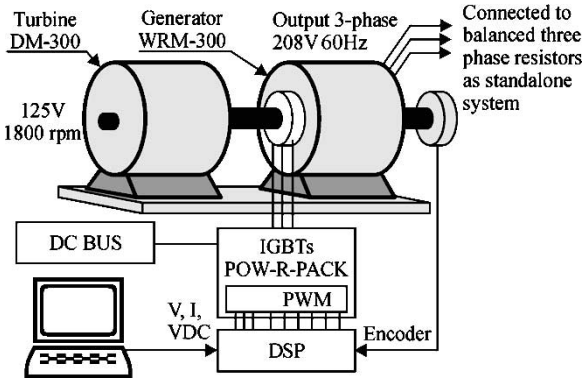

Fig. 11. Experimental system setup. In this setup, the main generator is a 3-hp three-phase wound-rotor induction machine; the turbine is simulated by a dc motor. The exciter is not included in the setup.

TABLE II
WIND TURBINE PROFILE AND EXCITER AND POWER CONVERTER POWER RATING

Speed (rpm)	Generator output	Rotor current(A)	Rotor voltage (V)	Exciter Power (kW)	Converter Power (kVA)
800	0.720	6.7	127	0.604	1.472
1000	1.296	7.5	106	0.816	1.381
1200	1.908	8.6	86	0.936	1.286
1500	2.232	9.3	52	0.698	0.834
1750	2.232	9.3	24	0.371	0.378
1800	2.232	9.3	19	0.305	0.305
1850	2.232	9.3	16	0.240	0.252
2000	2.160	9.1	19	0.042	0.305

The generator was set to have an output of 230 V and 60 Hz. The speed was varied from 800 to 2000 r/min, using the wind power profile given in Table II. The required current, voltage, and power for the rotor excitation were measured at different shaft speeds and compared to the calculated using the equivalent circuit.

Fig. 13 shows the measured stator voltage waveform. Fig. 14 shows the measured rotor voltage compared to the ones calculated using the equivalent circuit model. Fig. 15 shows the measured power supplied to the rotor winding for each given output of the stator. It is compared to the ones calculated by the equivalent model. Fig. 16 shows the measured rotor current versus the rotor current calculated by the equivalent circuit. It can be seen from the comparison of Fig. 14 to Fig. 15 that the measurements agree with simulations by the equivalent circuit.

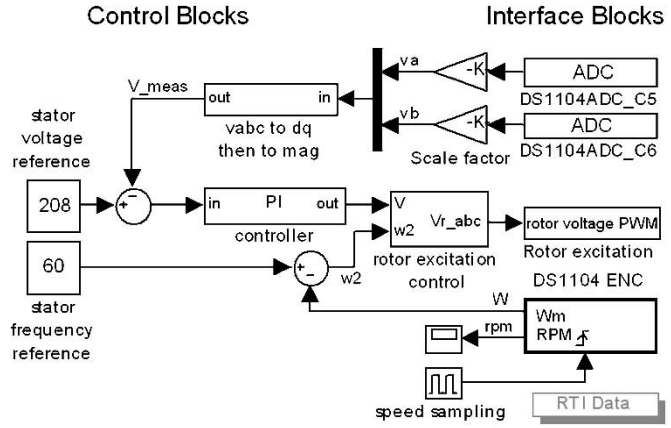

Fig. 12. Control implementation of a stand-alone generation system using dSPACE embedded real-time controller. In this setup, the stator voltage reference is set to 208 V and the stator frequency is set to 60 Hz.

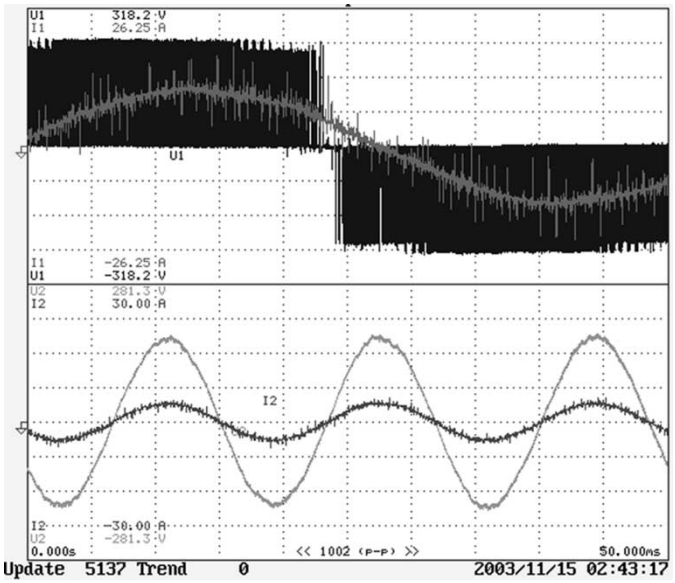

Fig. 13. Measurements of the generator at 1266 r/min. Upper: rotor voltage (PWM wave) and current (grey sine wave); lower: stator voltage (grey) and current (black). Stator voltage is 60 Hz, 120 V (phase), with pure resistive load of 42.8 Ω. It shows that although the rotor voltage is a PWM wave, the stator voltage and current are almost harmonic free.

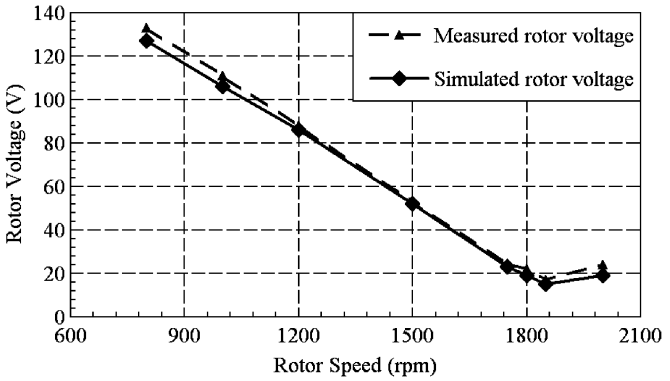

Fig. 14. Measured and calculated rotor voltage of the main generator. The output is set to 60 Hz and 230 V for any given rotor speed.

Although it is not implemented in this paper, it is possible to eliminate the encoder by using a frequency PID controller to control the stator frequency of a stand-alone system to eliminate the speed encoder.

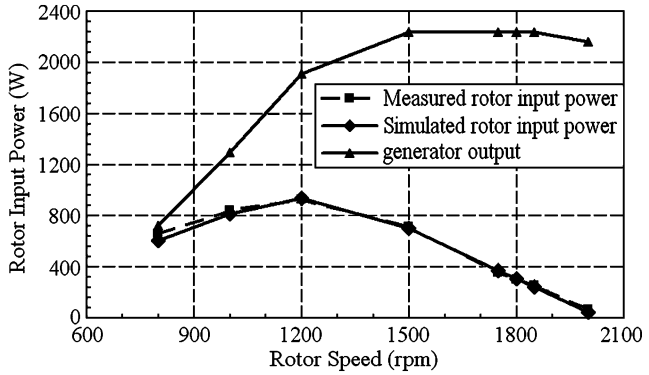

Fig. 15. Measured and experimented power of the stator and rotor. The output is set to 60 Hz and 230 V for any given rotor speed.

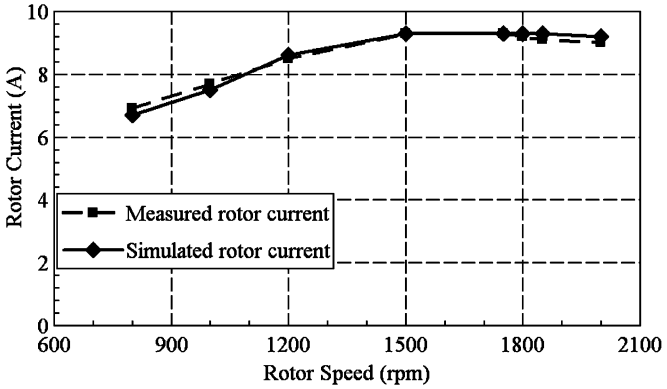

Fig. 16. Measured and calculated rotor current. The output is set to 60 Hz and 230 V for any given rotor speed.

The transient behavior of the generation system was not studied in this paper. However, the transients of the generation system were observed in the experiments. It was found that the transient process is generally smooth with a sudden change of speed when it is operated at subsynchronous speeds. At super-synchronous speeds, the stator frequency is not as stable as it is operated at subsynchronous speeds. When operated near synchronous speeds, it is also more difficult to maintain the stator voltage at constant due to the fact that the rotor excitation is almost dc.

VI. Conclusion

A novel variable-speed constant-frequency power generation system has been proposed and modeled. The experiment shows that the proposed system can produce a stable voltage and frequency at the main generator terminals for any given turbine speed. The advantages of the proposed system can be summarized as follows.

1) The system is capable of being a stand-alone system and self-var support. In the case of large wind systems, self starting and self stopping is achieved without the requirement of additional facilities, such as soft starters or braking systems.
2) The system provides improved power factor controllability and reduced line harmonic distortion, by eliminating the direct connection of a power converter to the power grid.

An equivalent circuit was developed to model the doubly fed induction generator incorporating stator and iron losses. While steady-state operation of the system has been modeled and verified by experiments, dynamic characteristics and stability of the system needs to be investigated.

The experimental study of a 3-kW prototype system, which includes the proposed generator, exciter, and a power converter, is in progress. Once successful it will eventually be transitioned to a megawatt wind power generation system.

Appendix

The Matlab simulation program for the equivalent circuit is as follows.

```
% equivalent circuit analysis of
% doubly-fed generator
% this program calculates the
% needed rotor voltage,
% current and power
% for required stator current and speed
% also calculates the system efficiency
% given speed and rotor current
n = [800 1000 1200 1500 1750 1800 1850 2000];
I = [2.0 3.6 5.3 6.2 6.2 6.2 6.2 6.0];
% define variables using symbols
syms r1 x1 rms rmr xm r2 x2 V1 I1m phi
syms s a rad pad Iad real;
I1 = I1m*exp(-i*phi);
E1 = V1 + I1*(r1 + i*x1);
Im = E1/(rms + rmr*s + i*xm);
I2 = (Im + I1)*a; V2 = s*E1/a + I2*(r2 + i*s*x2);
V1 = 120;     % Stator phase voltage
pmec = 111;   % windage and friction loss
pad = 81;     % stray load loss
a = 1.0;      % turns ratio
r1 = 0.41;    % stator resistance
x1 = 1.2;     % stator leakage inductance
r2 = 1.18;    % rotor resistance
x2 = 1.0;     % rotor leakage inductance
xm = 19.3;    % mutual inductance
rms = 0.63;   % stator iron loss component
rmr = 0.08;   % rotor iron loss component
phi = 0;      % stator phase angle (PF)
for  k = 1 : 8
   I1m = I(k);  s = ((1800 - n(k))/1800);
   R_cur = eval  (I2);
   I2_amp(k) = abs  (Rotor_current);
   R_volt = eval  (V2);
   V2_amp(k) = abs  (Rotor_voltage);
   Rotor_power(k) = 3*real  (R_volt*conj(R_cur))
   P1(k) = 3*V1*I1m;
   Converter_p(k) = 3*V2_amp(k)*I2_amp(k)/1000;
   Effi  (k) = 3*I1m*V1/(3*I1m*V1 + 3*I1m^2*r1+
   3*I2_amp(k)^2*r2 + 3*abs(eval(Im))^2*
   (rms + abs(s)*rmr) + pmec + pad)*100;
end
plot  (n, Effi, n, I2_amp, n, Rotor_power)
```

ACKNOWLEDGMENT

The authors would also like to thank N. Stranges from the Large Motors Division of General Electric Company for his valuable recommendations.

REFERENCES

[1] M. G. Simoes, B. K. Bose, and R. J. Spiegel, "Fuzzy logic based intelligent control of a variable speed cage machine wind generation system," *IEEE Trans. Power Electron.*, vol. 12, pp. 87–95, Jan. 1997.

[2] A. Grauers, "Efficiency of three wind energy generator systems," *IEEE Trans. Energy Conversion*, vol. 11, pp. 650–657, Sept. 1996.

[3] Y. Tang and L. Xu, "A flexible active and reactive power control strategy for a variable speed constant frequency generating system," *IEEE Trans. Power Electron.*, vol. 10, pp. 472–478, July 1995.

[4] S. Kato, N. Hoshi, and K. Oguchi, "A low cost system of variable speed cascaded induction generators for small-scale hydroelectricity," in *Conf. Rec. IEEE-IAS Annu. Meeting*, vol. 2, 30 Sep.–4 Oct. 2001, pp. 1419–1424.

[5] R. E. Betz and M. G. Jovanovic, "The brushless doubly-fed reluctance machine and the synchronous reluctance machine—a comparison," *IEEE Trans. Ind. Applicat.*, vol. 36, pp. 1103–1110, July/Aug. 2000.

[6] C. S. Brune, R. Spee, and A. K. Wallace, "Experimental evaluation of a variable speed, doubly-fed wind power generations system," *IEEE Trans. Ind. Applicat.*, vol. 30, pp. 648–654, May 1994.

[7] C. Concordia, S. B. Crary, and G. Kron, "The doubly-fed synchronous machines," *AIEE Trans.*, vol. 61, pp. 286–289, May 1942.

[8] B. M. Bird and R. F. Burbidge, "Analysis of doubly-fed slip ring machines," *Proc. Inst. Elect. Eng.*, vol. 113, pp. 1016–1020, June 1966.

[9] W. B. Gish, J. R. Schurz, B. Milano, and F. R. Schleif, "An adjustable speed synchronous machine for hydroelectric power applications," *IEEE Trans. Power App. Syst.*, vol. PAS-100, pp. 2171–2176, Nov. 1981.

[10] F. J. Brady, "A mathematic model for the doubly-fed wound rotor generator," *IEEE Trans. Power App. Syst.*, vol. 103, pp. 798–802, Apr. 1984.

[11] ——, "A mathematic model for the doubly-fed wound rotor generator—Part II," *IEEE Trans. Energy Conversion*, vol. 1, pp. 180–183, June 1986.

[12] M. Riaz, "Energy conversion properties of induction machines in variable speed constant frequency generating systems," *AIEE Trans.*, pt. II, vol. 8, pp. 25–30, Mar. 1959.

[13] M. S. Vicatos and J. A. Ieqopoulos, "Steady state analysis of a doubly-fed induction generator under synchronous operation," *IEEE Trans Energy Conversion*, vol. 4, pp. 495–501, Sept. 1989.

[14] J. Taaura, T. Sasaki, S. Ishikawa, and J. Hasegawa, "Analysis of the steady state characteristics of doubly-fed synchronous machines," *IEEE Trans Energy Conversion*, vol. 4, pp. 250–256, June 1989.

[15] M. Yamamoto and O. Motoyoshi, "Active and reactive power control for doubly-fed wound rotor induction generator," *IEEE Trans. Power Electron.*, vol. 6, pp. 624–629, Oct. 1991.

[16] T. Wildi, *Electrical Machines, Drives, and Power Systems*, 5th ed. Upper Sadle River, NJ: Prentice-Hall, 2002.

[17] C. Mi, J. Shen, and N. Natarajan, "Field-oriented control of induction motors," in *Proc. 2002 IEEE Workshop on Power Electronics in Transportation (WPET 2002)*, Auburn Hills, MI, Sept. 2002, pp. 69–73.

Chunting Mi (S'00–A'01–M'01–SM'03) received the B.S.E.E. and M.S.E.E. degrees from Northwestern Polytechnical University, Xi'an, China, and the Ph.D. degree from the University of Toronto, Toronto, ON, Canada, all in electrical engineering.

He is an Assistant Professor at the University of Michigan, Dearborn, with teaching responsibilities in the area of power electronics, electric vehicles, electric machines and drives. From 2000 to 2001, he was an Electrical Engineer with General Electric Canada Inc. He was responsible for designing and developing large electric motors and generators up to 30 MW. He began his career at the Rare-Earth Permanent Magnet Machine Institute of Northwestern Polytechnical University. He joined Xi'an Petroleum Institute as an Associate Professor and Associate Chair of the Department of Automation in 1994. He was a Visiting Scientist at the University of Toronto from 1996 to 1997. He has recently developed the Power Electronics and Electrical Drives Laboratory at the University of Michigan, Dearborn. His research interests are electric drives and power electronics; induction, brushless, and PM synchronous machines; renewable energy systems; and electrical and hybrid vehicle powertrain design and modeling.

Dr. Mi is the Chair of the Power and Industrial Electronics Chapter of the IEEE Southeast Michigan Section.

Mariano Filippa (S'03) received the B.S.M.E. degree from the Technological Institute of Buenos Aires (ITBA), Buenos Aires, Argentina. He is currently working toward the M.S. degree in automotive engineering at the University of Michigan, Dearborn.

He is also currently a Research Assistant at the University of Michigan, Dearborn, working at the DTE Power Electronics Laboratory. He is responsible for the design of power electronic converters and testing equipment for motor control applications and laboratory testing. From 2001 to 2002, he was an Application Engineer at Asea Brown Boveri, Buenos Aires, Argentina, working in the area of robotics. He had a key role in the engineering and construction of a fully automated robotized palletizing cell for the consumer industry. During 2002, he was also involved in R&D at the Technological Institute of Buenos Aires, designing a distributorless ignition system for laboratory research. His research interests are low- and medium-power electronics applications, ranging from control algorithms, EMI reduction, and equipment design and testing, in the areas of motor control and hybrid vehicle applications.

Mr. Filippa is a Student Member of the American Society of Mechanical Engineers.

John Shen received the B.S. degree from Tsinghua University, Beijing, China, in 1987, and the M.S. and Ph.D. degrees from Rensselaer Polytechnic Institute, Troy, NY, in 1991 and 1994, respectively, all in electrical engineering.

He is currently with the Department of Electrical and Computer Engineering, University of Michigan, Dearborn. Between 1994–1999, he was with Motorola Inc., Phoenix, AZ, where he held the position of Senior Principal Staff Engineer in the discrete-power semiconductor division. His current research interests include power semiconductor devices and ICs, power electronics, automotive electronics, automotive power systems, electromagnetic compatibility, sensors and actuators, and system reliability analysis. He has authored more than 50 journal and refereed conference publications, and eight issued and numerous pending U.S. patents in these areas.

Dr. Shen currently chairs the Technical Committee of Automotive Power Electronics, IEEE Power Electronics Society. He is a recipient of the 2003 U.S. National Science Foundation CAREER Award.

Narashim Natarajan received the B. Tech. degree from the Indian Institute of Technology, Madras, India, in 1974, and the M.S. and Ph.D. degrees from the University of California, Berkeley, in 1998 and 1999, respectively.

He is currently an Associate Professor in the Department of Electrical and Computer Engineering, University of Michigan, Dearborn. His research interests include robotics, intelligent systems, and computer security.